ORNL/TM-2024/3546

Method for Coupled Electromagnetic and Circuit Simulations to Evaluate Surge Arrester Performance in Protecting Equipment Against E1 HEMP

DaHan Liao
Yilu Liu
Lawrence C. Markel
Benjamin W. McConnell
Brian R. Poole
Lisa Wang

September 2024

OAK RIDGE National Laboratory

ORNL IS MANAGED BY UT-BATTELLE LLC FOR THE US DEPARTMENT OF ENERGY

ORNL/TM-2024/3546

Energy Science and Technology Directorate
Electrification and Energy Infrastructures Division

METHOD FOR COUPLED ELECTROMAGNETIC AND CIRCUIT SIMULATIONS TO EVALUATE SURGE ARRESTER PERFORMANCE IN PROTECTING EQUIPMENT AGAINST E1 HEMP

DaHan Liao
Yilu Liu
Lawrence C. Markel
Benjamin W. McConnell
Brian R. Poole
Lisa Wang

September 2024

Prepared by
OAK RIDGE NATIONAL LABORATORY
Oak Ridge, TN 37831
managed by
UT-Battelle LLC
for the
US DEPARTMENT OF ENERGY
under contract DE-AC05-00OR22725

CONTENTS

LIST OF FIGURES iv
LIST OF TABLES v
ABBREVIATIONS vi
ABSTRACT 1
1. INTRODUCTION 1
2. Simulation and Modeling Framework 2
    2.1 Linear Response Characterization in Frequency-Domain Electromagnetic Solver 4
    2.2 Circuit Response Characterization in Time-Domain SPICE Solver 4
3. RESULTS 5
4. SUMMARY 8
5. REFERENCES 15

LIST OF FIGURES

1 E1 HEMP illumination of a generic facility with a SCADA system connected to a surge-protected PLC. 2
2 PLC subsystem and cable network. 4
3 AutomationDirect DL06 Micro PLC for which Qiu et al. [1] carried out port impedance characterization. 5
4 SPICE-compatible circuit network for transient simulation. 7
5 Surge arrester model. 7
6 Induced open-circuit voltage at Port 1. 8
7 Induced short-circuit current at Port 1: (a) total and (b) common and differential modes. . . . 9
8 S-parameters for cable as calculated with MoM. 10
9 Comparison of cable input impedance at Port 1 calculated using MoM vs. an equivalent circuit model. 10
10 Comparison of PLC port impedance from measurements vs. an equivalent circuit model. . . 11
11 Comparison of load voltage derived from a full-wave solver and a hybrid solver. The protected load was a 100 Ω resistor. 11
12 Comparison of load voltage derived from a full-wave solver and a hybrid solver. The protected load was a PLC. 12
13 PLC load voltage under E1 HEMP illumination (a) without building attenuation and without a surge arrester; (b) without building attenuation and with a surge arrester; (c) with building attenuation and without a surge arrester; and (d) with building attenuation and with a surge arrester. Cable parameters: $L = 10$ m and $h = 1$ m. 13
14 PLC load voltage under E1 HEMP illumination (a) without building attenuation and without a surge arrester; (b) without building attenuation and with a surge arrester; (c) with building attenuation and without a surge arrester; and (d) with building attenuation and with a surge arrester. Cable parameters: $L = 10$ m and $h = 3$ m. 14

LIST OF TABLES

1 Parameters for I-V characteristics of $R_{bias,sa}$. 6

ABBREVIATIONS

DUT	device under test
FDTD	finite-difference time-domain
HEMP	high-altitude electromagnetic pulse
MoM	method of moments
ORNL	Oak Ridge National Laboratory
PLC	programmable logic controller
SCADA	Supervisory Control and Data Acquisition
SPICE	Simulation Program with Integrated Circuit Emphasis

ABSTRACT

Surge arrester behavioral modeling for realistic systems embedded in an E1 high-altitude electromagnetic pulse environment inherently encompasses three interconnected complications: (1) the need to account for signal propagation across two domains, electromagnetics and electrical; (2) the need to include both linear and nonlinear circuit components in the analysis; and (3) the need to understand that the over-current and over-voltage mitigation performance is dependent not only on the properties of the surge arrester and protected load but also on the topology of the overall electrical network. This study presents a framework to address these challenges in a systematic manner to consider the effectiveness of protective measures for a common class of equipment in power generation facilities. Full-wave simulations were carried out to derive circuit-domain (i.e., lumped element–based) equivalent models for the excitation waveform and the physical components of the system. Then, these equivalent models were imported to a circuit solver and combined with a high-frequency surge arrester model to evaluate mitigation performance. The methodology outlined is general enough such that it can be applied for other electromagnetic interference problems that involve E2/E3 HEMP or microwave emissions.

1. INTRODUCTION

Stakeholders in the bulk electric power sector are interested in addressing how to determine the coupling of high-intensity electromagnetic wave energy with power plant equipment and assessing its effects. Recently, two reports [2; 3] have been published as products of Oak Ridge National Laboratory's (ORNL's) research investment in this area, specifically pertaining to the E1 component of a high-altitude electromagnetic pulse (HEMP) as a stimulus. The first report [2] provides insights into the internal intensity levels that a typical power generation facility would experience under E1 HEMP illumination and introduces the concept of using a semi-empirical attenuation function to characterize the radio wave propagation channel. The authors performed a detailed analysis of the shielding effectiveness of building physical structures using both first-principles electromagnetic simulations and on-site measurement data. The second report [3] prescribes a new systematic approach (i.e., a four-step procedure) that combines measurement and modeling efforts for calculating the induced voltages and currents on the equipment ports. These two reports do not directly address the need to incorporate mitigation measures into the hybrid electrical–electromagnetics systems considered in the studies. As a follow-up investigation, the current report documents the additional technical and analysis framework required to close this gap.

This study contextualizes its objective around applications related to the Supervisory Control and Data Acquisition (SCADA) systems of a power generation plant (Figure 1), which play a fundamental role in the operation of the facility. Although their exact implementation differs depending on the plant type and infrastructure, these systems are highly computerized and, in general, consist of the following major sub-components [4; 5]: (1) a supervisory system (or central host server) for data processing and command execution; (2) programmable logic controllers (PLCs) and/or remote terminal units for direct control of, for example, sensors, actuators, switch boxes, and other field devices; (3) a communications network for transferring data between the supervisory system and the PLCs and remote terminal units; and (4) a human–machine interface and hardware/software components that provide operators with the ability to monitor and interact with the SCADA system.

The vulnerability of certain SCADA devices to HEMP has been partially investigated by previous works [1; 6; 7; 8; 9]. These studies assessed the effects of a fast, high-intensity pulse on the instrument by experimental or simulated injection testing without considering facility shielding and cable coupling.

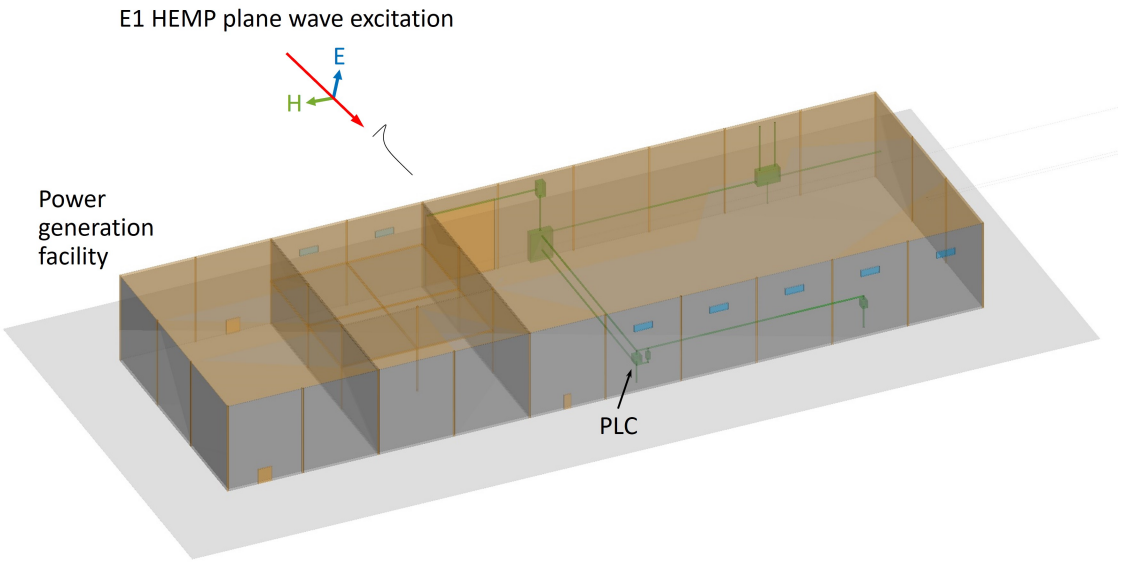

Figure 1. E1 HEMP illumination of a generic facility with a SCADA system connected to a surge-protected PLC.

Because the various ports of these components can be connected to long transmission lines (e.g., those attached to instrument power supply or communications devices), a need exists to understand how electromagnetic energy can penetrate into these systems through those ports. The amount of coupling is a function of myriad variables, including the location of the equipment within the facility, wire/cable length and geometrical configuration, wire/cable electrical properties, terminal loading position and impedance values, and orientation/direction of the excitation field. In this work, a simulation approach was developed to model the transients that propagate along the cable, the resultant port voltage/current waveforms that are generated, and the effectiveness of surge arresters in mitigating the energy surge. A salient feature in the numerical modeling methodology in this study is the development of a technique for the co-simulation of linear and nonlinear circuit/electromagnetics systems, which enables seamless tracking of external radio wave signals into the terminals of an arbitrary impedance load or surge arrester of interest.

Section 2 delineates the simulation and modeling framework for the treatment of hybrid linear–nonlinear, electrical–electromagnetics systems; Section 3 presents an example application to evaluate the effects of E1 HEMP on a SCADA PLC instrument; and Section 4 summarizes the study.

2. SIMULATION AND MODELING FRAMEWORK

Ideally, the entire electrical–electromagnetics system (transmission lines, building environment, and associated linear/nonlinear circuit networks) would be simulated in a full-wave solver such as method of moments (MoM) as implemented in Altair Feko [10]. However, even without considering the computational memory and runtime requirements, traditional MoM, which operates in the frequency domain, cannot handle nonlinear effects. Other full-wave numerical methods such as the finite-difference time-domain (FDTD) and finite element method can be considered. Theoretically, FDTD is ideal for nonlinear analysis since it is an explicit time-domain solver [11; 12]. Unfortunately, in existing commercial

software, the extension to include nonlinear circuit elements has either not been implemented (as in the case of Feko FDTD) or has been implemented in a limited manner (as in the case of Remcom XFDTD [13]). The application of time- and frequency-domain finite element method solvers such as ones from COMSOL Multiphysics [14] were also considered; however, simulation of coupled linear/nonlinear interactions in these codes encountered similar challenges as those of the other software packages mentioned.

Because of the deficiencies in existing full-wave capabilities, a hybrid approach was developed to obtain E1 HEMP responses of surge arresters and cable loads. The simulation framework involved decomposing the original problem into a two-step solution process: a linear one that is treated with an electromagnetic solver, and a nonlinear one that is treated with a Simulation Program with Integrated Circuit Emphasis (SPICE) solver. In the electromagnetic domain, for an external stimulus (e.g., plane wave), the frequency-domain open-circuit voltage (for a Thevenin equivalence) or short-circuit current (for a Norton equivalence) is calculated at the transmission line port where the surge arrester and protected load are to be placed. This step necessitates the use of a physical model for the transmission line and, when sufficient computational resources are available, the facility structure. In a separate electromagnetic simulation, the two-port S-parameters of the transmission line—which are needed to develop a lumped element–based model for the cable network—are also extracted by characterizing the wideband voltage/current responses when the system is excited with, for example, voltage sources.

Next, the quantities determined from the electromagnetic simulations were imported into a circuit solver for transient analysis including the surge arrester and the protected load. The excitation of the circuit model was determined by transforming the open-circuit voltage or the short-circuit current into a time-domain waveform.

The response of a transmission line can be simulated in various ways in a SPICE solver. When the line loading is matched to the transmission line's characteristic impedance, a simple resistor would suffice, and such an assumption is expected to be valid across all frequencies. For generalized loading configurations (and for cases in which the line is lossy or re-radiating), one approach is to use the built-in standard transmission line modules in the model [15]; however, most of these modules are not sufficiently wideband for the current application. A second approach is to synthesize custom lumped-element cascaded network models using the transmission line per unit length parameters [16]. This method, too, is more appropriate for narrow-band applications. Although wideband versions of this approach have been implemented, they cannot be readily applied to generalized problem scenarios [17; 18; 19]. A third method is to convert the transmission line equivalent impedance into Laplace transforms and then embed those directly in the SPICE model. This technique is simple to implement but may lead to transient simulation instabilities.

In view of the shortcomings of the described approaches for the treatment of transmission lines in time-domain simulations, a systematic technique was developed to synthesize wideband equivalent SPICE circuit models from the S-parameters of the transmission line. The advantages of this approach are that (1) it can be applied to a wide variety of cable types—as long as the cables consist structures that can be simulated by the electromagnetic solver; (2) the complex interactions (e.g., coupling effects) between the environment and the cable can be completely captured since a full-wave solver is used to obtain the S-parameters; and (3) the generated circuit model is compatible with any SPICE software since it is essentially a lumped element–based model.

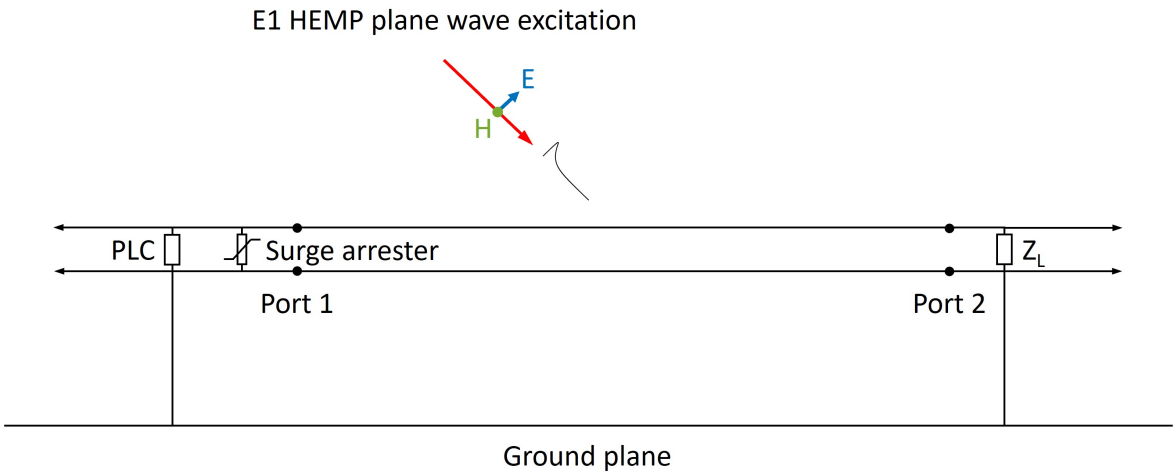

Figure 2. PLC subsystem and cable network.

2.1 LINEAR RESPONSE CHARACTERIZATION IN FREQUENCY-DOMAIN ELECTROMAGNETIC SOLVER

The PLC was assumed to be connected to one terminal of the cable network (e.g., power supply) as shown in Figure 2. The frequency-domain open-circuit voltage or short-circuit current at Port 1 was computed by simulating the structure with an MoM solver in which the excitation was provided by a plane wave with an E1 HEMP spectrum. Common and differential mode responses were simultaneously captured in this approach.

Next, equivalent SPICE circuit models were generated for the PLC and the cable network. This was accomplished by first approximating the frequency-domain admittance response (or Y-parameters) as a summation of rational functions with poles and residues and then transforming each of those functions into a lumped-element circuit representation. The standard procedure for carrying out this step is detailed elsewhere [20; 21; 22; 23; 24; 25]. In this work, the MATLAB routine `fit` was applied to obtain the rational function expansion, and the routine `generate` was applied to obtain the circuit derivation (that is, the SPICE netlist file). The PLC S-parameters were calculated from the measured impedance of the device [1], whereas for the cable network, those parameters were derived from two-port MoM simulations.

2.2 CIRCUIT RESPONSE CHARACTERIZATION IN TIME-DOMAIN SPICE SOLVER

The device under test (DUT) model, the cable network circuit model, and the excitation signal obtained from electromagnetic characterizations were imported into a SPICE solver [26] for time-domain simulations to examine the equipment response in the presence of a surge arrester. Although the focus of the study is on surge arresters, the same simulation framework can be applied to analyze any nonlinear component that may need to be incorporated into the model. Furthermore, no restrictions exist on the type of excitation signal that can be treated using this procedure; E1 HEMP is of primary interest here, but the other HEMP components (i.e., E2 and E3 [27; 28]), as well as intentional electromagnetic interferences [29], can be included as the stimulus.

For equipment located inside the facility, to account for signal attenuation due to the building structure, the open-circuit voltage or short-circuit current spectrum from Section 2.1 was multiplied with a

Figure 3. AutomationDirect DL06 Micro PLC for which Qiu et al. [1] carried out port impedance characterization.

semi-empirical transfer function derived by Liao et al. [2] before it was transformed to the time domain. Different locations within a facility may have different attenuation profiles; in this example, the transfer function used corresponded to the one experienced by a signal that was propagating into the control room of the power plant characterized by Liao et al. [2]. As noted by Liao et al. [2], the attenuation trends observed through measurements demonstrated good agreement with those obtained using numerical simulations.

Various surge arrester models have been developed for the treatment of lightning (microsecond timescales) impulses [30; 31; 32]. However, these models are not valid for E1 HEMP analysis, which requires capturing transient response dynamics at nanosecond timescales. Without losing generality, the model applied in this work was parameterized from manufacturer data and measurements carried out by Bowman et al. [33]. The clamping voltage of the employed surge arrester was higher than necessary for the protection of the SCADA equipment of interest; nevertheless, it is still helpful in demonstrating the modeling and simulation framework.

3. RESULTS

This section presents a generic example to illustrate the steps in simulating the response of a PLC (i.e., the DUT displayed in Figure 3) with and without surge arrester protection.

In this example, the cable had length $L = 10$ m, and the height above the ground plane was $h = 1$ m. The load at Port 2 was taken to be constant with an impedance of 100 Ω, though an arbitrary (frequency-dependent) load could be included in a similar manner. Emulating an E1 HEMP stimulus, as shown in Figure 2, the excitation was a vertically polarized plane wave impinging from an incidence angle of $\theta_i = 45°$, with the incident electric field vector set to be parallel to the geometrical plane containing the cable wires.

Figures 6 and 7(a) show the induced open-circuit voltage and short-circuit current, respectively, at Port 1 as a function of frequency (for a plane wave with unity amplitude). Figure 7(b) shows a breakdown of the current into common and differential modes. These two modal currents, I_{cm} and I_{dm}, are defined as

$$\begin{bmatrix} I_{cm} \\ I_{dm} \end{bmatrix} = \begin{bmatrix} 1 & 1 \\ \frac{1}{2} & -\frac{1}{2} \end{bmatrix} \begin{bmatrix} I_u \\ I_l \end{bmatrix} \tag{1}$$

where I_u and I_l are the currents on the upper and lower wire branches of the ports, respectively. As expected, the dominant coupling component was caused by the common mode current. Figure 8 shows the simulated two-port S-parameters of the cable, and Figure 10 shows the measured impedance of the DUT.

Table 1. Parameters for I-V characteristics of $R_{bias,sa}$.

Parameter	Value
a	39.70 GΩ
b	48.407
c	152.73 kV
d	27.98 Ω
e	6.149
f	279.81 kV

The overall SPICE-compatible circuit network that was simulated is displayed in Figure 4. The network includes the wideband equivalent circuit models (for the cable and DUT) and a ZnO metal-oxide varistor surge arrester model (Figure 5) from Bowman et al. [33]. The metal-oxide varistor model was defined by the following: $L_{sa} = 1.218$ µH, $C_{sa} = 16.4$ pF, and the I-V curve for $R_{bias,sa}$ given as

$$I = \frac{V}{\frac{a}{1+\left(\frac{V}{c}\right)^b} + \frac{d}{\left(\frac{V}{f}\right)^e}} \tag{2}$$

The values for the parameters are listed in Table 1.

To verify the validity of the derived equivalent circuit models, the SPICE-simulated input impedances were compared with reference solutions obtained from the MoM solver for the cable or from measurements for the DUT; as demonstrated in Figures 9 and 10, good agreement was observed between the two data sets. Next, before adding the surge arrester to the model, MoM and equivalent circuit solutions for the unprotected transient load voltage response at Port 1 were obtained and are shown in Figure 11 for a 100 Ω load, and in Figure 12 for a PLC load. For both loading configurations, the hybrid solution closely followed the "exact" full-wave solution. The periodicity of the late-time response corresponded to the fundamental resonance of the cable.

Figure 13 shows the PLC transient load voltage (a) without building attenuation and without a surge arrester; (b) without building attenuation and with a surge arrester; (c) with building attenuation and without a surge arrester; and (d) with building attenuation and with a surge arrester. In this example, the facility (control room) provided significant added protection, as structural shielding can attenuate the peak voltage by a factor of ~18 for the case without a surge arrester, and ~24 for the case with a surge arrester. The surge arrester employed, as expected, could not lower the induced load voltage, given its high cramping voltage rating. However, additional distortions in the response were observed when the surge arrester was included in the model.

After the response at the PLC port was determined, the next step was to assess how the equipment would be affected. Experimental testing of the SCADA equipment through pulse injection is beyond the scope of the work; therefore, where appropriate, published upset and damage values for comparable equipment were applied as reference points to evaluate device health. For instance, according to the fast pulse testing results presented by Savage et al. [6], for PLCs, depending on the port, upset can happen at a voltage as low as 1.6 kV, and damage can happen at as low as 0.6 kV. A computer/network switch was also tested, and the results indicate that upset can occur at 2.0 kV, and damage at 0.5 kV. Furthermore, testing on digital protection relays has indicated that "failures and operational disorders" can occur at 3.2–3.3 kV [34]. Based on these findings from literature and the simulated response results from this study, the PLC of

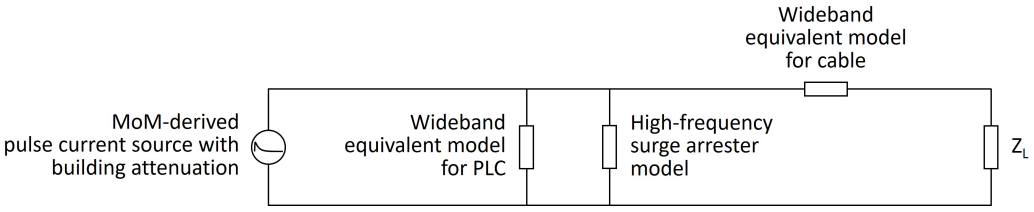

Figure 4. SPICE-compatible circuit network for transient simulation.

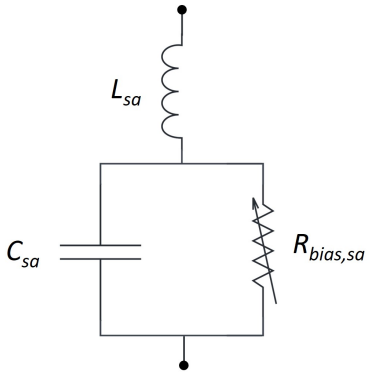

Figure 5. Surge arrester model.

interest in this work would likely be damaged for a scenario without building shielding but could only be potentially upset or damaged when it is located inside the facility.

As noted, the induced port voltage amplitude is dependent on the cable geometry. At frequencies for which the cable loop size (i.e., common mode loop circumference) is small compared with the wavelength, the response is expected to increase with increasing frequency. However, the amplitude would not increase monotonically and would reach saturation around the 10–40 m range [3; 35]. As a second example, the voltage response of the network configuration from Figure 2 with h = 3 m is shown in Figure 14. Given the larger loop size, a higher peak voltage was observed compared with the case with h = 1 m, demonstrating increased device vulnerability.

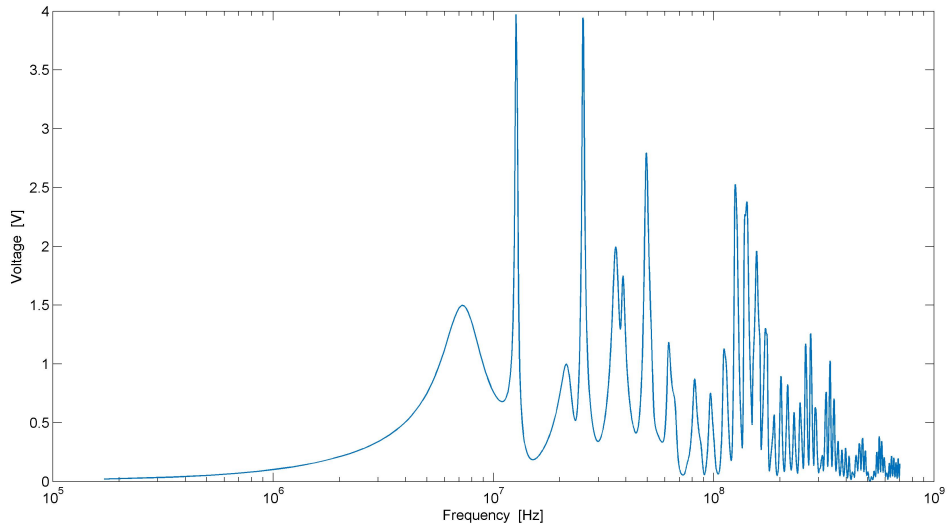

Figure 6. Induced open-circuit voltage at Port 1.

4. SUMMARY

When analyzing power system radiated susceptibility for E1 HEMP applications, electromagnetic coupling and facility attenuation effects are often not directly considered. Existing works largely follow a heuristic approach in which the stimulus is simply modeled as a standard voltage or current source. In view of the lack of a systematic modeling and simulation approach for evaluating the effectiveness of protection devices against fast, high-intensity transients, a hybrid framework is presented in this study that seamlessly and accurately connects the dynamics in the electromagnetics domain with those in the electrical circuit domain—all while retaining the ability to incorporate both linear and nonlinear components into the model. The generality of the approach, which employs both simulation and empirical data, allows for arbitrary cable types, electronics equipment, and electromagnetic environments to be included in the analysis. As an example of the practicality of the proposed technique in assessing the vulnerability of a SCADA system under E1 HEMP illumination, the response of a surge-protected PLC was characterized.

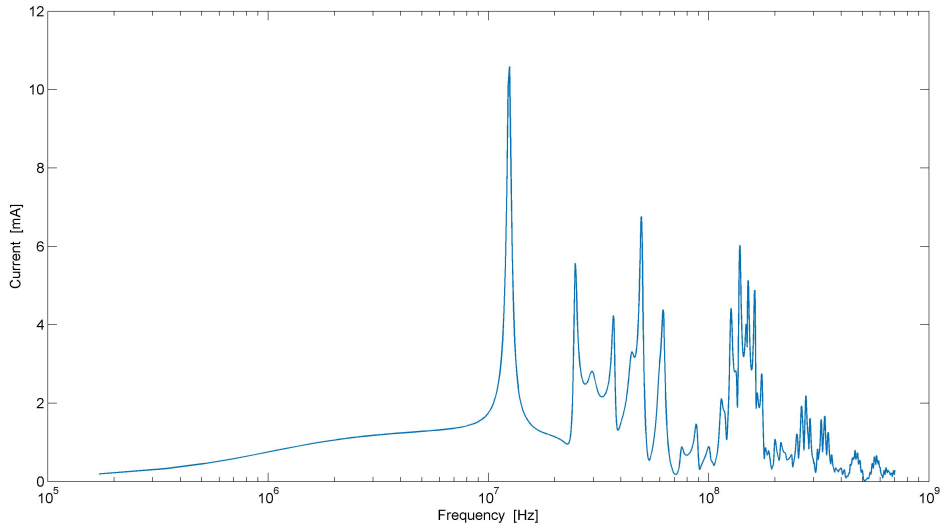

(a)

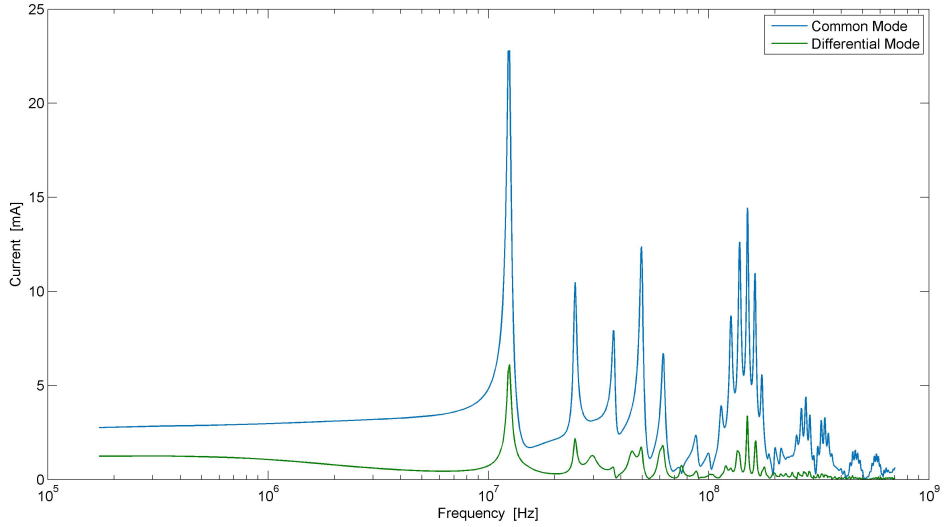

(b)

Figure 7. Induced short-circuit current at Port 1: (a) total and (b) common and differential modes.

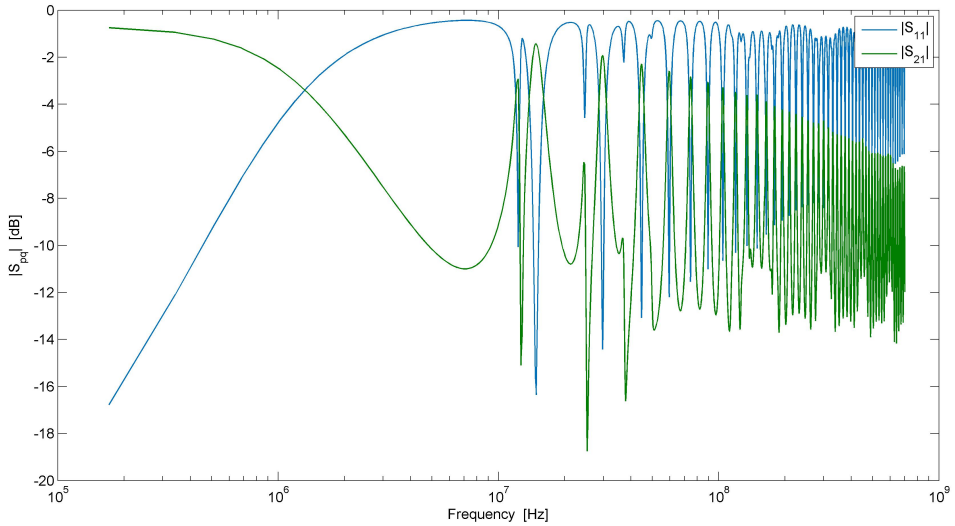

Figure 8. S-parameters for cable as calculated with MoM.

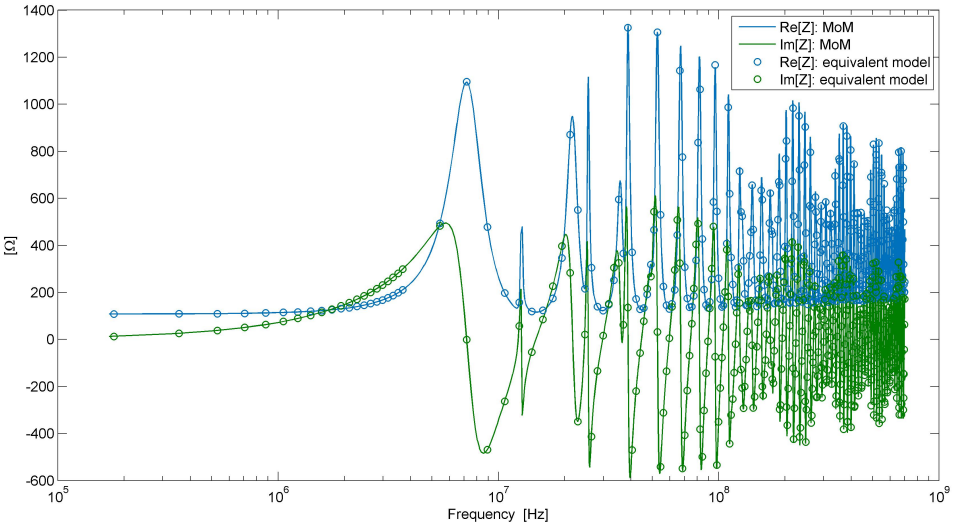

Figure 9. Comparison of cable input impedance at Port 1 calculated using MoM vs. an equivalent circuit model.

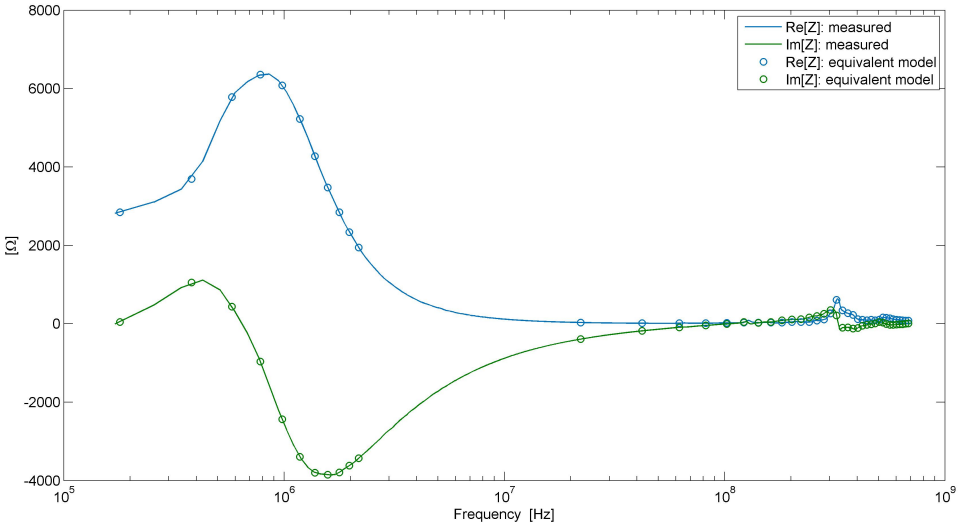

Figure 10. Comparison of PLC port impedance from measurements vs. an equivalent circuit model.

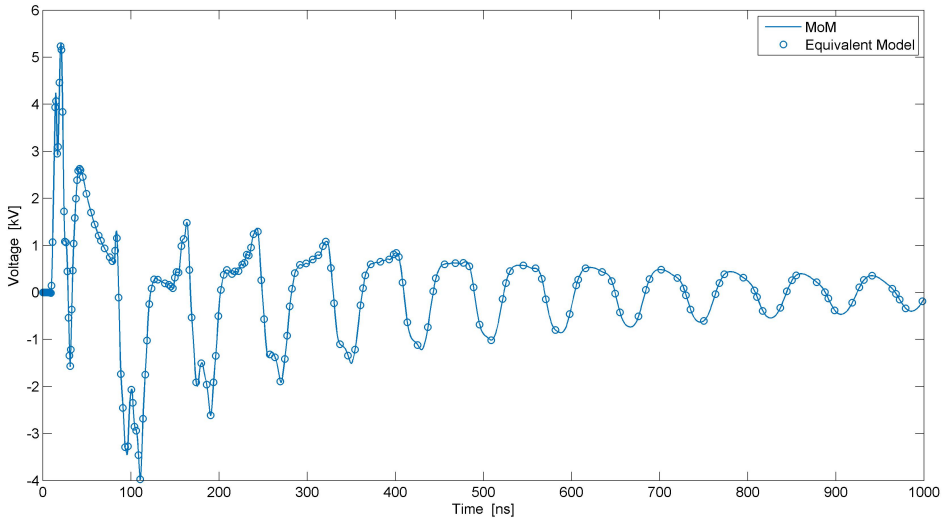

Figure 11. Comparison of load voltage derived from a full-wave solver and a hybrid solver. The protected load was a 100 Ω resistor.

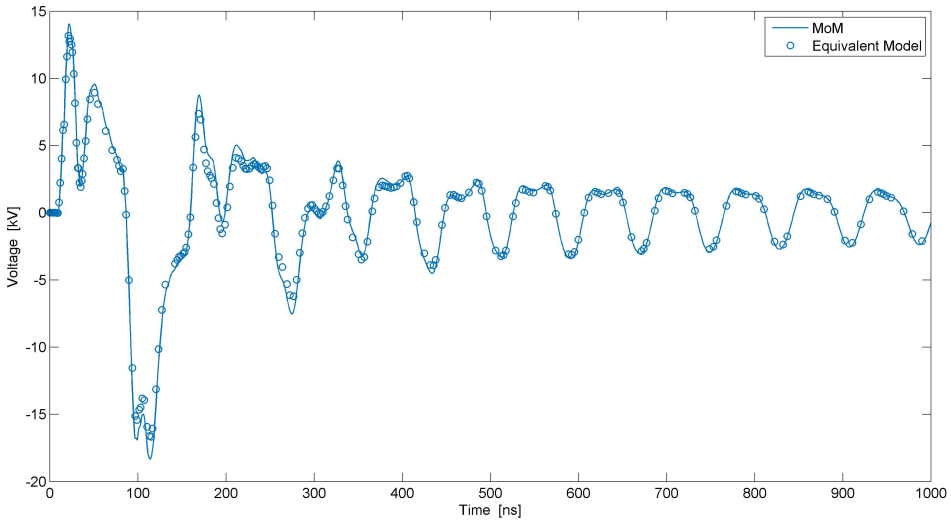

Figure 12. Comparison of load voltage derived from a full-wave solver and a hybrid solver. The protected load was a PLC.

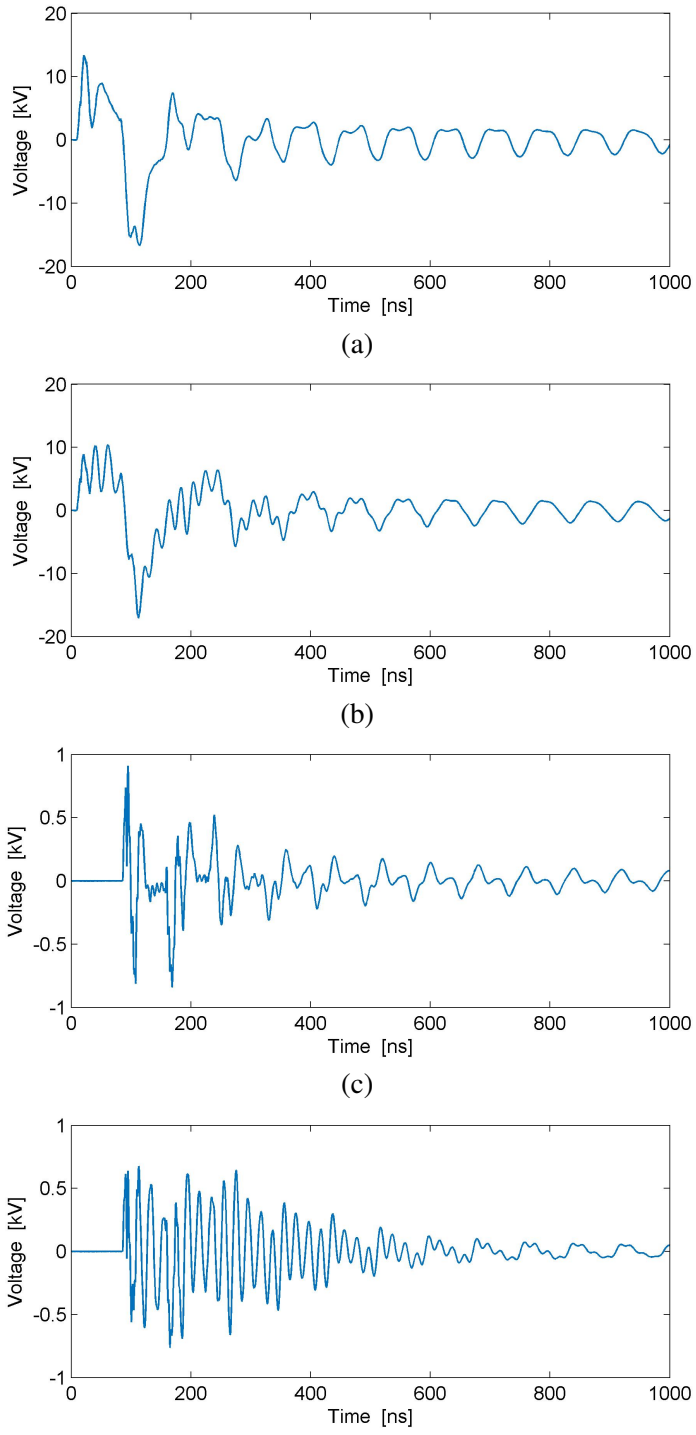

Figure 13. PLC load voltage under E1 HEMP illumination (a) without building attenuation and without a surge arrester; (b) without building attenuation and with a surge arrester; (c) with building attenuation and without a surge arrester; and (d) with building attenuation and with a surge arrester. Cable parameters: $L = 10$ **m and** $h = 1$ **m.**

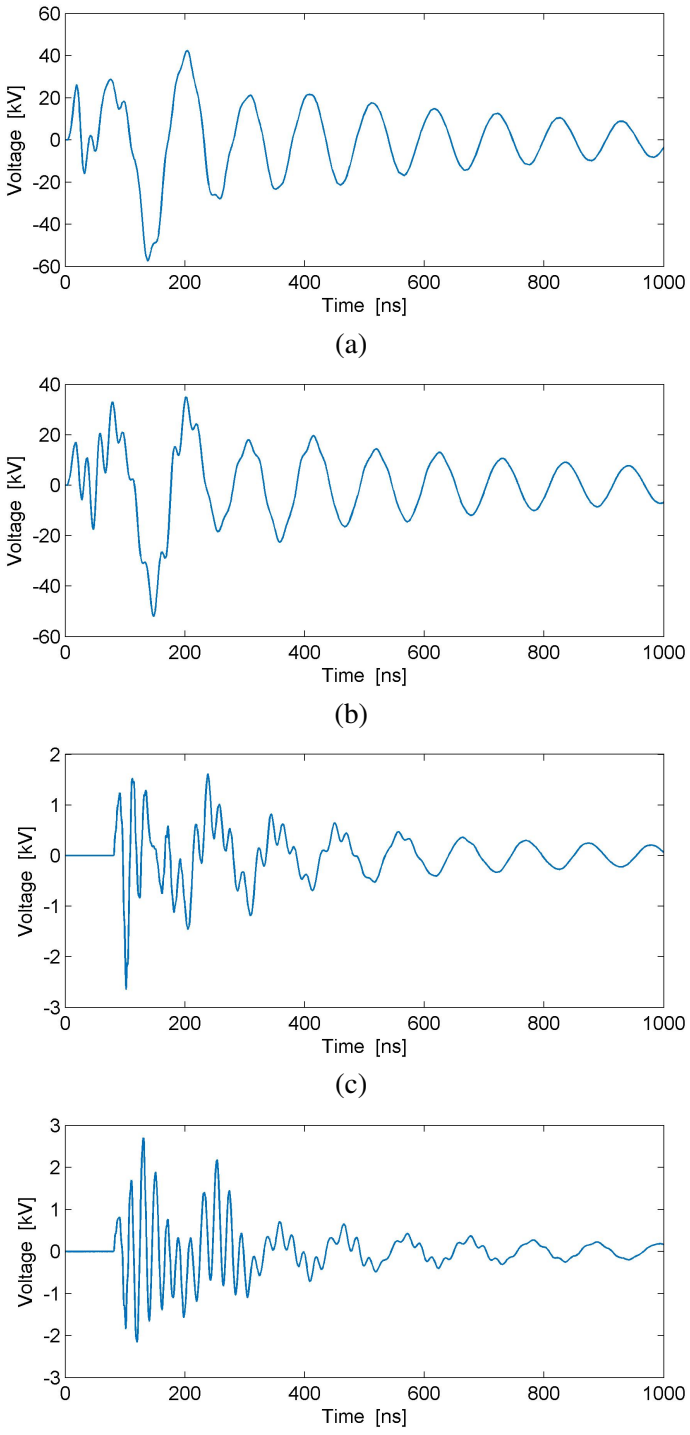

Figure 14. PLC load voltage under E1 HEMP illumination (a) without building attenuation and without a surge arrester; (b) without building attenuation and with a surge arrester; (c) with building attenuation and without a surge arrester; and (d) with building attenuation and with a surge arrester. Cable parameters: $L = 10$ **m and** $h = 3$ **m.**

5. REFERENCES

[1] W. Qiu, L. Zhang, H. Yin, K. Sun, L. Markel, D. Liao, Z. Li, B. McConnell, and Y. Liu, "Port impedance measurement and current injection response analysis for PLCs," *IEEE Transactions on Industry Applications*, vol. 58, no. 6, pp. 7,838–7,846, 2022.

[2] D. Liao, Z. Li, Y. Liu, L. Markel, B. McConnell, B. Poole, and L. Wang, "Estimation of high-altitude electromagnetic pulse signal leakage into power generation facilities: Simulations and measurements," Tech. Rep. ORNL/TM-2022/2779, Oak Ridge National Laboratory, 2022.

[3] D. Liao, Y. Liu, L. Markel, B. McConnell, D. Mignardot, B. Poole, and L. Wang, "A systematic approach for estimating high-altitude electromagnetic pulse coupling onto power generation facility equipment," Tech. Rep. ORNL/TM-2023/2997, Oak Ridge National Laboratory, 2023.

[4] M. Lakhoua, "SCADA applications in thermal power plants," *International Journal of the Physical Sciences*, vol. 5, pp. 1175–1182, 2010.

[5] R. Kumar, M. Dewal, and K. Saini, "Utility of SCADA in power generation and distribution system," in *2010 3rd International Conference on Computer Science and Information Technology*, vol. 6, pp. 648–652, 2010.

[6] E. Savage, J. Gilbert, and W. Radasky, "The early-time (E1) high-altitude electromagnetic pulse (HEMP) and its impact on the U.S. power grid," Tech. Rep. Meta-R-320, 2010.

[7] W. Qiu, L. Zhang, H. Yin, K. Sun, L. Markel, D. Liao, Z. Li, B. McConnell, and Y. Liu, "PLC-based impedance measurement and current injection response analysis," in *2021 IEEE Industry Applications Society Annual Meeting (IAS)*, pp. 1–6, 2021.

[8] L. Zhang, W. Qiu, H. Yin, K. Sun, L. Markel, D. Liao, Z. Li, B. McConnell, and Y. Liu, "Immunity study: Port impedance measurement of PMU and PCI testing under EMP," in *2022 IEEE/IAS Industrial and Commercial Power System Asia (ICPS Asia)*, 2022.

[9] L. Zhang, W. Qiu, H. Yin, L. Markel, D. Liao, B. McConnell, and Y. Liu, "Voltage and current response characteristics of PMU device by PCI simulation," in *2022 IEEE International Conference on High Voltage Engineering and Applications (ICHVE)*, pp. 1–4, 2022.

[10] Altair, "Feko," 2024. https://www.altair.com/feko/.

[11] Y.-C. Mei, X.-L. Wu, Z.-X. Huang, S.-L. Lu, X.-G. Ren, and H.-M. Du, "Simulation of nonlinear hybrid circuit by FDTD," in *2012 International Conference on Microwave and Millimeter Wave Technology (ICMMT)*, vol. 5, pp. 1–3, 2012.

[12] C.-N. Kuo, B. Houshmand, and T. Itoh, "Full-wave analysis of packaged microwave circuits with active and nonlinear devices: an FDTD approach," *IEEE Transactions on Microwave Theory and Techniques*, vol. 45, no. 5, pp. 819–826, 1997.

[13] Remcom, "XFDTD," 2024. https://www.remcom.com/xfdtd-3d-em-simulation-software.

[14] COMSOL, "COMSOL multiphysics," 2024. https://www.comsol.com/comsol-multiphysics.

[15] C. May, *Transmission Lines*, pp. 417–444. Cham: Springer International Publishing, 2020.

[16] C. R. Paul, *Analysis of Multiconductor Transmission Lines*. John Wiley & Sons, 2007.

[17] R. McCammon, "SPICE simulation of transmission lines by the Telegrapher's method - Part 1: Putting the Telegrapher's equations into a circuit," *EETimes*, 2010.

[18] R. McCammon, "SPICE simulation of transmission lines by the Telegrapher's method - Part 2: Putting frequency dependence into the simulation," *EETimes*, 2010.

[19] R. McCammon, "SPICE simulation of transmission lines by the Telegrapher's method - Part 3: Putting the Telegrapher's equations into a usable sub-circuit," *EETimes*, 2010.

[20] B. Gustavsen and A. Semlyen, "Rational approximation of frequency domain responses by vector fitting," *IEEE Transactions on Power Delivery*, vol. 14, no. 3, pp. 1052–1061, 1999.

[21] B. Gustavsen, "Improving the pole relocating properties of vector fitting," *IEEE Transactions on Power Delivery*, vol. 21, no. 3, pp. 1587–1592, 2006.

[22] A. Morched, B. Gustavsen, and M. Tartibi, "A universal model for accurate calculation of electromagnetic transients on overhead lines and underground cables," *IEEE Transactions on Power Delivery*, vol. 14, no. 3, pp. 1032–1038, 1999.

[23] B. Gustavsen, "Wide band modeling of power transformers," *IEEE Transactions on Power Delivery*, vol. 19, no. 1, pp. 414–422, 2004.

[24] G. Antonini, "SPICE equivalent circuits of frequency-domain responses," *IEEE Transactions on Electromagnetic Compatibility*, vol. 45, no. 3, pp. 502–512, 2003.

[25] D. Liao, "A hybrid approach for characterizing linear and nonlinear electromagnetic scattering: Theory and applications," Tech. Rep. ARL-TR-6261, US Army Research Laboratory, 2012.

[26] Analog-Devices, "LTspice," 2024. https://www.analog.com/en/resources/design-tools-and-calculators/ltspice-simulator.html.

[27] S. K. Pukkalla and B. Subbarao, "Evaluation of critical point-of-entry (POE) protection devices for E1 E2 pulses as per MIL STD 188-125-12," in *2018 15th International Conference on ElectroMagnetic Interference Compatibility (INCEMIC)*, pp. 1–4, 2018.

[28] S. Kim and I. Jeong, "Vulnerability assessment of korean electric power systems to late-time (E3) high-altitude electromagnetic pulses," *Energies*, vol. 12, no. 17, 2019.

[29] W. Radasky, C. Baum, and M. Wik, "Introduction to the special issue on high-power electromagnetics (HPEM) and intentional electromagnetic interference (IEMI)," *IEEE Transactions on Electromagnetic Compatibility*, vol. 46, no. 3, pp. 314–321, 2004.

[30] IEC60099-4, "Surge arresters–part 4: Metal-oxide surge arresters without gaps for ac systems," 2014.

[31] P. Pinceti and M. Giannettoni, "A simplified model for zinc oxide surge arresters," *IEEE Transactions on Power Delivery*, vol. 14, no. 2, pp. 393–398, 1999.

[32] F. Fernandez and R. Diaz, "Metal oxide surge arrester model for fast transient simulations," in *Proceedings of 2001 International Conference on Power System Transients*, pp. 681–687, 2001.

[33] T. Bowman, M. Halligan, and R. Llanes, "High-frequency metal-oxide varistor modeling response to early-time electromagnetic pulses," in *2020 IEEE International Symposium on Electromagnetic Compatibility & Signal/Power Integrity (EMCSI)*, pp. 466–471, 2020.

[34] V. Gurevich, "Resilience of digital protection relays to electromagnetic pulse (HEMP)," 2017.

[35] C. Du, Z. Cui, C. Mao, X. Nie, S. Zheng, and W. Wang, "Response characteristic analysis of long dipole antennas excited by HEMP waves," in *2021 Computing, Communications and IoT Applications (ComComAp)*, pp. 107–111, 2021.